INTERNATIONAL JOURNAL OF ROBUST AND NONLINEAR CONTROL
Int. J. Robust. Nonlinear Control 2013; **23**:919–931
Published online 2 April 2012 in Wiley Online Library (wileyonlinelibrary.com). DOI: 10.1002/rnc.2809

An iterative algorithm for maximizing robust performance in $\mathscr{H}_\infty$ loop-shaping design

M. Osinuga[1,*,†], S. Patra[2] and A. Lanzon[1]

[1]*Control Systems Centre, School of Electrical and Electronic Engineering, The University of Manchester, Sackville Street, Manchester M13 9PL, United Kingdom*
[2]*Department of Electrical Engineering, Indian Institute of Technology Kharagpur 721302, India*

SUMMARY

In this paper, an algorithm that gives the best achievable performance bound on a given control problem is proposed using the $\mathscr{H}_\infty$ loop-shaping design framework. In view of standard design requirements, the robust performance is maximized at low and high frequencies while keeping the robust stability margin above a specified level, and the robust stability margin is directly improved at mid frequencies (around crossover). The proposed frequency-dependent optimization problem is cast in an LMI framework. The resulting solution algorithm simultaneously synthesizes loop-shaping weights and a stabilizing controller that achieve the maximum performance for a given level of robust stability margin corresponding to sufficient gain and phase margins of the closed-loop system. Copyright © 2012 John Wiley & Sons, Ltd.

Received 10 June 2011; Revised 5 December 2011; Accepted 31 January 2012

KEY WORDS: $\mathscr{H}_\infty$ loop-shaping; robust performance; robust stability margin; weight optimization; LMI

1. INTRODUCTION

The so-called $\mathscr{H}_\infty$ loop-shaping design procedure (LSDP) [1] is a well-known robust control design methodology that combines classical loop-shaping concepts with $\mathscr{H}_\infty$ synthesis. This procedure establishes a good trade-off between robust performance and robust stability of a closed-loop system in a systematic framework. The closed-loop design objectives in different frequency regions are specified in terms of the loop-gain of the compensated system, for example, input disturbance rejection/attenuation and reference signal tracking at low frequencies, stability and damping improvement around the crossover, insensitivity to sensor noise and unmodeled plant dynamics at high frequencies, and so on. The philosophy of this design procedure is to maximize the robust stability margin for a given performance. On the contrary, this paper proposes a 'reversed' paradigm where the performance is maximized for a given level of robust stability margin, and this is of great significance to the practicing community. To show the relevance of this 'reversed' paradigm, a physically motivated example is given.

We consider a single-input single-output plant whose transfer function is given as

$$G(s) = 0.2\frac{\left(s^2 + 2\zeta_1\omega_1 s + \omega_1^2\right)\left(s^2 + 2\zeta_2\omega_1 s + \omega_1^2\right)}{\left(s^2 + 2\zeta_1\omega_2 s + \omega_2^2\right)\left(s^2 + 2\zeta_2\omega_2 s + \omega_2^2\right)},$$

where $\omega_1 = 0.2115$, $\omega_2 = 0.0473$, $\zeta_1 = 0.3827$, and $\zeta_2 = 0.9239$ [2]. This plant, formed by cascading two second-order lag-lead Butterworth filters with two lightly damped modes, has been

*Correspondence to: M. Osinuga, Control Systems Centre, School of Electrical and Electronic Engineering, The University of Manchester, Sackville Street, Manchester M13 9PL, United Kingdom.

†E-mail: mobolaji.osinuga-2@postgrad.manchester.ac.uk

widely studied (see, for example, [3, 4]). This filter has a practical application in the broad field of digital signal processing and conditioning, for example, in audio processing and oceanographic records [5]. For this plant, a controller is designed to achieve a good tracking performance as well as attenuate low frequency disturbance signals in the presence of actuator saturation, which is an inherent feature of most control systems. In view of these objectives, it is worth designing a controller that maximizes the closed-loop performance while also guaranteeing some level of stability margin. This will thus ensure that a satisfactory level of performance is retained when the system is operating in the saturation zone, even though the performance is degraded. Now, we adopt the $\mathscr{H}_\infty$ LSDP to synthesize a controller for the aforementioned plant using the following cases:

Case 1: If pre-compensators and post-compensators are chosen as the identity and the corresponding $\mathscr{H}_\infty$ loop-shaping controller is synthesized, a robust stability margin of 0.4592 is obtained.

Case 2: On the other hand, if the loop-gain at low (resp. high) frequencies is maximized (resp. minimized) (as depicted in Figure 1(a)) by selecting the pre-compensator as $3500\frac{s+0.1}{(s+2.5)^3}$ and fixing the post-compensator as the identity, a robust stability margin of 0.4478 is obtained when the corresponding $\mathscr{H}_\infty$ loop-shaping controller is synthesized.

The closed-loop system responses (V_{out}) to a unit step input voltage (V_{in}) using these controllers with saturation of ± 1 are shown in Figure 1(b). The performance in terms of the settling time, 'undershoot', and steady-state error is all better in Case 2 despite the fact that both controllers have similar robust stability margin.

In view of the aforementioned scenario, a designer will therefore be interested to know what can or cannot be achieved performance-wise on a particular problem when a pre-specified level of stability margin is demanded. In this paper, a novel approach using the $\mathscr{H}_\infty$ loop-shaping framework is employed to maximize the robust performance of a closed-loop system for a given and guaranteed level of robust stability margin. The philosophy casts a frequency-dependent optimization problem that respectively improves the robust stability margin around the crossover and, for a guaranteed level of robust stability margin, maximizes both robust performance at low frequencies and robustness to unmodeled dynamics and unpredicted sensor noise, and so on, at high frequencies. This is thus an optimized approach to a closed-loop system design where priority is placed on performance, stability, and robustness at low, mid, and high frequencies, respectively. The proposed optimization problem builds on the framework established in [6, 7] and is formulated in a quasiconvex [8] form to provide an easy and systematic solution to the designer. The resulting solution to the optimization problem simultaneously synthesizes a robustly stabilizing controller and loop-shaping weights.

The rest of the paper is organized as follows. Notations are defined in Section 2, whereas a brief description on the $\mathscr{H}_\infty$ LSDP's concept and the weight optimization problem of [6, 7] are given in Section 3 as background of the present work. The standard design objectives and the corresponding

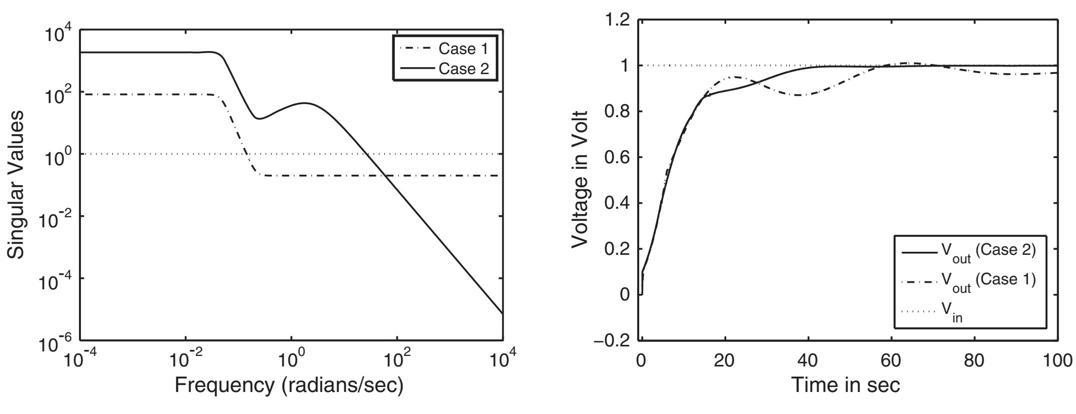

Figure 1. (a) Singular values of the shaped plant and (b) unit step response with actuator saturation.

DOI: 10.1002/rnc

formulations in LMI framework that capture the introduced philosophy are given in Sections 4 and 5, respectively. The solution algorithm is detailed in Section 6, and in Section 7, a numerical example is shown to justify the philosophy of the proposed algorithm. Section 8 concludes the paper.

2. NOTATION

Notation is standard. $\mathbb{R}$, $\mathbb{R}_+$, and $\mathbb{R}_+^n$ denote, respectively, the set of real numbers, strictly positive real numbers, and column vectors of dimension $(n \times 1)$, with each entry belonging to $\mathbb{R}_+$. $\mathscr{R}^{n\times m}$ and $\mathscr{RH}_\infty^{n\times m}$ are the set of real rational and real rational stable transfer function matrices with dimension $(n \times m)$, respectively. Functions that are units in $\mathscr{RH}_\infty$ are said to belong to $\mathscr{GH}_\infty$, that is, $f \in \mathscr{GH}_\infty \Leftrightarrow f, f^{-1} \in \mathscr{RH}_\infty$. $\operatorname{diag}\begin{pmatrix} a \\ b \end{pmatrix}$ is a shorthand notation for $\begin{pmatrix} a & 0 \\ 0 & b \end{pmatrix}$. The i-th singular value of matrix A is represented as $\sigma_i(A)$, and the condition number is defined as $\kappa(A) := \overline{\sigma}(A)/\underline{\sigma}(A)$, where $\overline{\sigma}(A)$ (resp. $\underline{\sigma}(A)$) is the largest (resp. smallest) singular value of matrix A. A^* is the complex conjugate transpose of matrix A. For compactness of notation, we define the following set:

$$\mathbf{\Pi}(\alpha,\beta,\zeta,\eta) := \{W = \operatorname{diag}\begin{pmatrix} w_1 \\ w_2 \\ \vdots \\ w_p \end{pmatrix} \in \mathscr{GH}_\infty^{p\times p} : \alpha(\omega) < \sigma_i(W(j\omega)) < \beta(\omega), \kappa(W(j\omega)) < \zeta(\omega),$$

$$\left| \frac{d}{d(\log_{10}\omega)} (20\log_{10}|w_i(j\omega)|) \right| < \eta(\omega)\ \forall \omega, i = 1, 2, \ldots, p\}$$

for some given continuous real-valued frequency functions $\alpha, \beta, \zeta, \eta : \mathbb{R} \to \mathbb{R}_+$ that satisfy $\beta(\omega) > \alpha(\omega)$, $\zeta(\omega) > 1$, and $\eta(\omega) > 0\ \forall\omega$. Moreover, let $\mathbf{\Lambda_n}$ represent the set of real strictly positive diagonal matrices of dimension $(n \times n)$, defined as $\mathbf{\Lambda_n} := \{\operatorname{diag}(x) : x \in \mathbb{R}_+^n\}$.

3. BRIEF OVERVIEW OF WEIGHT OPTIMIZATION IN THE $\mathscr{H}_\infty$ LOOP-SHAPING DESIGN PROCEDURE

In this section, we describe briefly the $\mathscr{H}_\infty$ LSDP (depicted in Figure 2(a)) and the weight optimization framework of [7] for underpinning the concepts and mathematical machinery of the present work. If the feedback interconnection in Figure 2(a) is denoted as $[P_s, C_\infty]$ and $\mathscr{C}(P)$ represents the set of all stabilizing controllers for a plant P, that is, $\mathscr{C}(P) = \{C : [P, C] \text{ is internally stable}\}$, the robust stability margin of $[P_s, C_\infty]$ is then defined as

$$b(P_s, C_\infty) := \begin{cases} \left\| \begin{bmatrix} P_s \\ I \end{bmatrix} (I - C_\infty P_s)^{-1} \begin{bmatrix} -C_\infty & I \end{bmatrix} \right\|_\infty^{-1} & \text{if } C_\infty \in \mathscr{C}(P_s) \\ 0 & \text{otherwise,} \end{cases} \tag{1}$$

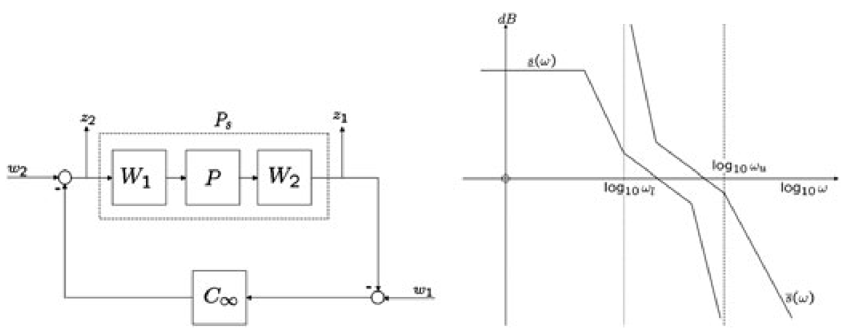

Figure 2. (a) $\mathscr{H}_\infty$ loop-shaping design framework and (b) typical loop-shape boundary.

DOI: 10.1002/rnc

and the maximum achievable robust stability margin is denoted as $b_{\text{opt}}(P_s) := \sup_{C_\infty} b(P_s, C_\infty) \in [0, 1]$. In this design framework, a stabilizing controller C_∞ is synthesized for the shaped plant $P_s = W_2 P W_1$ such that the robust stability margin of the feedback interconnection is maximized. The final $\mathscr{H}_\infty$ loop-shaping controller is subsequently obtained by cascading weights with the stabilizing controller C_∞ as $C = W_1 C_\infty W_2$. The significance of the robust stability margin, more importantly its pointwise-in-frequency equivalent around crossover, is illustrated in [9, Theorem 1.20] to indicate the size of the largest $\mathscr{H}_\infty$-norm bounded perturbation of the normalized coprime factors of P_s for which closed-loop stability is guaranteed. Consequently, maximizing the robust stability margin will effectively increase the robustness of the feedback interconnection to perturbations on the plant. It should be noted that the coprime factor uncertainty representation is arguably the most general type of unstructured uncertainty as it allows low/high frequency modeling errors and an unknown number of right-half plane poles and zeros.

In the first step, a designer's main task is to select 'good' weights W_1 and W_2 such that the shaped plant P_s is compatible with the performance requirements. Typically, they are chosen such that P_s has large gain at low frequencies, small gain at high frequencies, and does not roll off at a high rate around the crossover. This is depicted in Figure 2(b), where the region between $\underline{s}(\omega)$ and $\overline{s}(\omega)$ represents the permissible region for the desired loop-shape, selected on the basis of performance specifications.

However, it is known that the selection of weights is non-trivial [1, 6, 10–12]. The issues regarding weight selection have been discussed in detail in [1, 6, 12, 13], and in [6], all the design constraints are combined into a single optimization framework that simultaneously synthesizes weights and a stabilizing controller while maximizing the robust stability margin for a given performance. This work has been extended in [7] by formulating smoothness constraints on the gradient of the synthesized weights to avoid undesirable lightly damped 'approximate' pole-zero cancelations and is described next. Before describing this optimization framework, we define some useful terms that will be required to describe the algorithm and subsequent formulations. Denote γ as $\frac{1}{b(P_s, C_\infty)}$, and define the pointwise-in-frequency robust stability margin at a frozen frequency ω as $\rho_\omega(P_s, C_\infty) := b(P_s(j\omega), C_\infty(j\omega))$. Also, for a given plant $P \in \mathscr{R}^{m\times n}$, define $\Lambda_{1\omega} = W_1(j\omega)^{-*} W_1(j\omega)^{-1} \in \mathbf{\Lambda_n}$ and $\Lambda_{2\omega} = W_2(j\omega)^* W_2(j\omega) \in \mathbf{\Lambda_m}$.

The weight optimization framework of [7] is now stated as follows:
for a scaled plant $P \in \mathscr{R}^{m\times n}$, where[‡] $m \geqslant n$,

$$\max_{\substack{W_1 \in \mathbf{\Pi}(\underline{w}_1, \overline{w}_1, k_1, g_1) \\ W_2 \in \mathbf{\Pi}(\underline{w}_2, \overline{w}_2, k_2, g_2)}} b_{\text{opt}}(P_s)$$

subject to

$$\underline{s}(\omega) < \sigma_i(P_s(j\omega)) < \overline{s}(\omega) \ \forall i, \omega.$$

$\underline{s}$, $\overline{s}$, $\underline{w}_i$, $\overline{w}_i$, k_i, and g_i are frequency functions specified by the designer for loop-shaping weight $W_i(j\omega)(i = 1, 2)$. The aforementioned optimization problem seeks to maximize $b_{\text{opt}}(P_s)$ and therefore does not depend on any particular controller. With the use of the definition of $b(P_s, C_\infty)$ in (1) and by performing several algebraic manipulations, the aforementioned optimization problem was formulated in [7] at each frequency grid-point ω_q as follows, where $q = 1, 2, \ldots, N$ and N is selected by the designer, and $\delta\nu := \log_{10}\omega_q - \log_{10}\omega_{q-1}\ \forall q > 1$.

Minimize $\gamma^2_{\omega_q}$ such that $\exists C \in \mathscr{C}(P), \Lambda_{1\omega_q} \in \mathbf{\Lambda_n}, \Lambda_{2\omega_q} \in \mathbf{\Lambda_m}$ satisfying

$$\underline{s}(\omega_q)^2 \Lambda_{1\omega_q} < P^*(j\omega_q)\Lambda_{2\omega_q} P(j\omega_q), \tag{2a}$$

$$P^*(j\omega_q)\Lambda_{2\omega_q} P(j\omega_q) < \overline{s}(\omega_q)^2 \Lambda_{1\omega_q}, \tag{2b}$$

[‡]If this condition is not satisfied, a dual problem to that shown in Figure 2(a) where $W_1 = W_2^T, W_2 = W_1^T, P = P^T$, and $C_\infty = C_\infty^T$ would be considered.

DOI: 10.1002/rnc

$$\begin{aligned}&\begin{bmatrix} 0 & P(j\omega_q) \\ 0 & I \end{bmatrix}^* \begin{bmatrix} \Lambda_{2\omega_q} & 0 \\ 0 & \Lambda_{1\omega_q} \end{bmatrix} \begin{bmatrix} 0 & P(j\omega_q) \\ 0 & I \end{bmatrix} \\ &\leqslant \gamma_{\omega_q}^2 \begin{bmatrix} I & P(j\omega_q) \\ C(j\omega_q) & I \end{bmatrix}^* \begin{bmatrix} \Lambda_{2\omega_q} & 0 \\ 0 & \Lambda_{1\omega_q} \end{bmatrix} \begin{bmatrix} I & P(j\omega_q) \\ C(j\omega_q) & I \end{bmatrix},\end{aligned} \tag{2c}$$

$$\exists \underline{\xi}_{1\omega_q}, \overline{\xi}_{1\omega_q} : \underline{\xi}_{1\omega_q} I < \Lambda_{1\omega_q} < \overline{\xi}_{1\omega_q} I, \overline{w}_1(\omega_q)^{-2} < \underline{\xi}_{1\omega_q}, \overline{\xi}_{1\omega_q} < \underline{w}_1(\omega_q)^{-2}, \ \overline{\xi}_{1\omega_q} < k_1(\omega_q)^2 \underline{\xi}_{1\omega_q}, \tag{2d}$$

$$\exists \underline{\xi}_{2\omega_q}, \overline{\xi}_{2\omega_q} : \underline{\xi}_{2\omega_q} I < \Lambda_{2\omega_q} < \overline{\xi}_{2\omega_q} I, \underline{w}_2(\omega_q)^{2} < \underline{\xi}_{2\omega_q}, \ \overline{\xi}_{2\omega_q} < \overline{w}_2(\omega_q)^{2}, \ \overline{\xi}_{2\omega_q} < k_2(\omega_q)^2 \underline{\xi}_{2\omega_q}, \tag{2e}$$

$$0 < \begin{bmatrix} \frac{\ln 10}{10} \Lambda_{1\omega_{q-1}} g_1(\omega_q)\, \delta\nu & \left(\Lambda_{1\omega_q} - \Lambda_{1\omega_{q-1}}\right) \\ \left(\Lambda_{1\omega_q} - \Lambda_{1\omega_{q-1}}\right) & \frac{\ln 10}{10} \Lambda_{1\omega_{q-1}} g_1(\omega_q)\, \delta\nu \end{bmatrix} \text{ when } q > 1, \tag{2f}$$

$$0 < \begin{bmatrix} \frac{\ln 10}{10} \Lambda_{2\omega_{q-1}} g_2(\omega_q)\, \delta\nu & \left(\Lambda_{2\omega_q} - \Lambda_{2\omega_{q-1}}\right) \\ \left(\Lambda_{2\omega_q} - \Lambda_{2\omega_{q-1}}\right) & \frac{\ln 10}{10} \Lambda_{2\omega_{q-1}} g_2(\omega_q)\, \delta\nu \end{bmatrix} \text{ when } q > 1. \tag{2g}$$

This optimization problem is quasiconvex when the controller $C \in \mathscr{C}(P)$ is held fixed in (2c); $\Lambda_{i\omega_q}$ and $\overline{\xi}_{i\omega_q}\ \forall i = 1, 2$ are the decision variables. For simplicity of argument, diagonal weights are considered in the aforementioned optimization problem, which is a specialization of the (possibly) full non-diagonal weight formulation in [6], obtained by replacing unitary matrices with the identity matrix. This is consistent with the observation that diagonal loop-shaping weights are generally sufficient to shape the singular values of the nominal plant [11]. However, with minor modifications discussed in [6], it is easy to compute non-diagonal weights. Here, (2a) and (2b) delimit the singular values of the shaped plant P_s within the specified loop-shape boundaries $\underline{s}(\omega_q)$ and $\overline{s}(\omega_q)$, whereas (2c) captures the cost function that maximizes $b(P_s, C_\infty)$. In addition, (2d) and (2e) provide bounds on the singular values and condition numbers of the synthesized loop-shaping weights. LMI constraints (2f) and (2g) ensure smoothness in the magnitude response of the weights by restricting the gradient at each frequency grid-point ω_q with respect to ω_{q-1} within specified bounds $g_1(\omega_q)$ and $g_2(\omega_q)$.

4. PROBLEM FORMULATION

For the sake of simplicity in describing a single non-convex multi-objective optimization problem, the design objectives are divided into three parts, one each for the low frequency, mid frequency, and high frequency regions. The frequency division is based on the loop-shape boundary shown in Figure 2(b). Note that the chosen lower and upper frequencies ω_l and ω_u are problem-specific, and a prior knowledge on disturbance characteristics, modeling uncertainties, sensor noise, and so on, is needed to choose these values. A simple rule[§] of thumb can also be made as follows: $\omega_l = \frac{\omega_B}{10}$ and $\omega_u = 10\omega_B$, where ω_B is the desired bandwidth of the closed-loop system.

Because of the paramount importance of the robust stability around crossover (i.e., maximizing the gain and phase margins to avoid a perturbed plant encircling the Nyquist point), the pointwise-in-frequency robust stability margin is maximized without worrying about 'performance' at mid frequencies. Moreover, the extent to which $\underline{s}(\omega)$ can be maximized for given plant dynamics indicates how small the sensitivity transfer function matrix can possibly be made. A designer seeks to make the loop-gain large at low frequencies in order to obtain small sensitivity functions. Also, the objective at high frequencies is to make the complementary sensitivity transfer function matrix close to zero for good robustness by minimizing the loop-gain.

[§]When using this rule of thumb, some allowances must be incorporated such that desired objectives in frequency should not be too close to ω_l and ω_u because of contrasting design objectives around these boundary frequencies.

DOI: 10.1002/rnc

In view of the aforementioned considerations, the three design objectives can be stated as follows:

(i) $\forall\omega \in [\omega_l, \omega_u]$ (mid frequencies): maximize the pointwise-in-frequency robust stability margin ρ_ω without restricting the loop-shape, that is,

Given P and $C \in \mathscr{C}(P)$,

$$\max_{\substack{W_1 \in \mathbf{\Pi}(\underline{w}_1, \overline{w}_1, k_1, g_1) \\ W_2 \in \mathbf{\Pi}(\underline{w}_2, \overline{w}_2, k_2, g_2)}} \rho_\omega\left(W_2(j\omega)P(j\omega)W_1(j\omega), W_1^{-1}(j\omega)C(j\omega)W_2^{-1}(j\omega)\right); \quad (3)$$

(ii) $\forall\omega < \omega_l$ (low frequencies): maximize robust performance by maximizing the loop-gain $\underline{s}(\omega)$ of the compensated system P_s for a given robust stability margin $\bar{\epsilon} \in (0, 1)$, that is,

Given $\bar{\epsilon}$, P and $C \in \mathscr{C}(P)$,

$$\max_{\substack{W_1 \in \mathbf{\Pi}(\underline{w}_1, \overline{w}_1, k_1, g_1) \\ W_2 \in \mathbf{\Pi}(\underline{w}_2, \overline{w}_2, k_2, g_2)}} \underline{s}(\omega) \quad (4)$$

subject to
(a) $\underline{s}(\omega) < \sigma_i\left(W_2(j\omega)P(j\omega)W_1(j\omega)\right)$ $\forall i$ and
(b) $\bar{\epsilon} < \rho_\omega\left(W_2(j\omega)P(j\omega)W_1(j\omega), W_1^{-1}(j\omega)C(j\omega)W_2^{-1}(j\omega)\right)$;

(iii) $\forall\omega > \omega_u$ (high frequencies): maximize robustness by minimizing the loop-gain $\overline{s}(\omega)$ of the shaped plant P_s for a given robust stability margin $\bar{\epsilon} \in (0, 1)$, that is,

Given $\bar{\epsilon}$, P and $C \in \mathscr{C}(P)$,

$$\min_{\substack{W_1 \in \mathbf{\Pi}(\underline{w}_1, \overline{w}_1, k_1, g_1) \\ W_2 \in \mathbf{\Pi}(\underline{w}_2, \overline{w}_2, k_2, g_2)}} \overline{s}(\omega) \quad (5)$$

subject to
(a) $\sigma_i\left(W_2(j\omega)P(j\omega)W_1(j\omega)\right) < \overline{s}(\omega)$ $\forall i$ and
(b) $\bar{\epsilon} < \rho_\omega\left(W_2(j\omega)P(j\omega)W_1(j\omega), W_1^{-1}(j\omega)C(j\omega)W_2^{-1}(j\omega)\right)$.

5. OPTIMIZATION PROBLEMS IN LMI FRAMEWORK FOR THE THREE FREQUENCY REGIONS

By considering the design objectives stated in the previous section, we now formulate the optimization problems of interest pointwise-in-frequency, with q representing the index of the grid points. In all subsequent formulations, the framework given in (2a)–(2g) will be used.

(i) For the mid frequency region, that is, $\omega \in [\omega_l, \omega_u]$, the problem statement given in (3) can be recast into the following quasiconvex optimization problem at each $\omega_q \in [\omega_l, \omega_u]$:
Given P and $C \in \mathscr{C}(P)$,
Minimize $\gamma^2_{\omega_q}$ such that $\exists \Lambda_{1\omega_q} \in \mathbf{\Lambda_n}, \Lambda_{2\omega_q} \in \mathbf{\Lambda_m}$ satisfying LMI constraints (2c)–(2g).
LMI constraints (2a) and (2b) are not included as robust stability is prioritized over nominal performance in this frequency region.

(ii) Also, for the low frequency region, that is, $\omega < \omega_l$, the optimization problem given in (4) can be recast into the following pointwise-in-frequency quasiconvex optimization problem:
Given $\bar{\epsilon} \in (0, 1)$, P and $C \in \mathscr{C}(P)$, and at each $\omega_q < \omega_l$,
Minimize $\underline{s}(\omega_q)^{-2}$ such that $\exists \Lambda_{1\omega_q} \in \mathbf{\Lambda_n}, \Lambda_{2\omega_q} \in \mathbf{\Lambda_m}$ satisfying (2a), (2c)–(2g), and where γ_{ω_q} is fixed at $\bar{\epsilon}^{-1}$ in (2c). (2b) is not included in the aforementioned optimization problem as the loop-gain is being maximized from below.

DOI: 10.1002/rnc

(iii) Similarly, the optimization problem in the high frequency region, that is, $\omega > \omega_u$, given in (5) is equivalent to the following pointwise-in-frequency quasiconvex optimization problem:
Given $\bar{\epsilon} \in (0, 1)$, P and $C \in \mathscr{C}(P)$, and at each $\omega_q > \omega_u$,
Minimize $\bar{s}(\omega_q)^2$ such that $\exists \Lambda_{1\omega_q} \in \mathbf{\Lambda_n}, \Lambda_{2\omega_q} \in \mathbf{\Lambda_m}$ satisfying LMI constraints (2b)–(2g) with γ_{ω_q} fixed at $\bar{\epsilon}^{-1}$ in (2c). Equation (2a) is not included as the loop-gain is being minimized from above.

Remark 1
A number of standard closed-loop design objectives discussed in [1, 6, 13] are specified in terms of bound on some specific transfer functions that are function of the shaped plant, the robust stability margin, and singular values and condition numbers of the weights. Hence, constraints on the singular values and condition numbers of the loop-shaping weights must be enforced at all frequencies to constrain the bound on these transfer functions. It should be noted that these constraints, alongside those on the gradients of the loop-shaping weights, ((2d)–(2g)) are all active at all frequencies in the aforementioned formulations.

6. SOLUTION ALGORITHM

On the basis of the formulations given in the previous section, a sub-optimal solution algorithm is now proposed. Similar to *D-K* iterations and other solution methods for these types of optimizations [13–16], an iterative algorithm must be used to solve the proposed optimization problems because the posed problems are not simultaneously convex in all variables. Moreover, because there are three optimization problems to be solved, a systematic procedure must be employed such that there is no discontinuity or violation of constraints at the boundaries of the resulting solutions to each optimization problem. In fact, the following should be noted before presenting the solution algorithm:

(i) Typically, designers use W_1 and W_2 to shape the loop-gain at low and high frequencies, respectively, [17]. Hence, solutions to the optimization problems at low and high frequencies can be made to follow this general design practice by keeping W_2 and W_1 fixed at low and high frequencies, respectively.
(ii) Robust stability can easily be lost near the crossover [9]. Thus, we insist that the optimization problem at mid frequencies be solved before those at low and high frequencies. To avoid discontinuity of the resulting solutions at the boundaries of the frequency regions, low frequency and high frequency optimizations use the boundary values of the mid frequency optimization solution to seed their search.
(iii) Monotonic improvement in performance (resp. robustness) at low (resp. high) frequencies requires the magnitude values of the weights at ω_l and ω_u (i.e., magnitude values of the shaped plant P_s at ω_l and ω_u) to be constrained by the magnitude values of the weight obtained at these boundary frequencies in the previous iteration of the mid frequency optimization. This is needed because of contrasting design objectives of two adjacent frequency points at ω_l and ω_u; for example, the objective at $\omega_q = \omega_l$ is to maximize $\rho_{\omega_q}(P_s, C_\infty)$, whereas the objective at ω_{q-1} is to maximize $\underline{s}(\omega_{q-1})$ for a fixed $\bar{\epsilon}$.

Inputs to the algorithm

- A scaled nominal plant $P \in \mathscr{R}^{m \times n}$,
- Frequency functions $\underline{w}_i(\omega)$, $\overline{w}_i(\omega)$, $k_i(\omega)$, and $g_i(\omega)$ that delimit the allowable region for the singular values, condition number, and gradient of loop-shaping weight W_i $(i = 1, 2)$, and
- ω_l and ω_u that are used to divide frequencies into three distinct regions.

We denote each frequency grid point as ω_q, where $q = 1, 2, \ldots, n_l, \ldots, n_u, \ldots, N$ and also denote ω_{n_l} and ω_{n_u} as ω_l and ω_u, respectively, that is, $\omega_q \forall q = 1, \ldots, n_l - 1$ corresponds to the low frequency optimization, ω_q $\forall q = n_l, \ldots, n_u$ corresponds to the mid frequency optimization, and ω_q $\forall q = n_u + 1, \ldots, N$ corresponds to the high frequency optimization.

DOI: 10.1002/rnc

The algorithm[¶]

1. Given $\bar{\epsilon} \in (0, 1)$, specified by the designer based on prior knowledge of the plant/uncertainty or using $\bar{\epsilon} = 0.3$, which is equivalent to a closed-loop system's gain and phase margins greater than or equal to 5.39 dB and 34.92°, respectively, [18]. Find an initial controller $C_0^\star$ as a feasible starting point for the algorithm such that $\left[W_{2,0}^\star P W_{1,0}^\star, W_{1,0}^{-1\star} C_0^\star W_{2,0}^{-1\star}\right]$ is internally stable and $b(W_{2,0}^\star P W_{1,0}^\star, W_{1,0}^{-1\star} C_0^\star W_{2,0}^{-1\star}) \geqslant \bar{\epsilon}$ for some $W_{1,0}^\star, W_{2,0}^\star \in \mathcal{GH}_\infty$ (see Remark 3 on how to choose these initializing quantities). Set $i = 0$, where i denotes the iteration number, and let $\varepsilon_{max,0}^\star = -1$.
2. Increment i by 1.
3. (i) Solve the following quasiconvex optimization problem at each frequency grid point $\omega_q \in [\omega_{n_l}, \omega_{n_u}]$, where $q = n_l, n_l + 1, \ldots, n_u$:
   Minimize $\gamma_{\omega_q,i}^2$ such that $\exists \Lambda_{1\omega_q} \in \mathbf{\Lambda_n}, \Lambda_{2\omega_q} \in \mathbf{\Lambda_m}$ satisfying
   (a) (2c)–(2g), where $\gamma_{\omega_q}^2$ is replaced by $\gamma_{\omega_q,i}^2$ in (2c), and (2f) and (2g) are only active when $q > n_l$,
   (b) $\theta_{i-1}^2 \Lambda_{1\omega_{n_l}} < P^*(j\omega_{n_l}) \Lambda_{2\omega_{n_l}} P(j\omega_{n_l})$ when $i > 1$ and where $\theta_{i-1} = \underline{\sigma}\left(W_{2,i-1}(j\omega_{n_l}) P(j\omega_{n_l}) W_{1,i-1}(j\omega_{n_l})\right)$,
   (c) $P^*(j\omega_{n_u}) \Lambda_{2\omega_{n_u}} P(j\omega_{n_u}) < \phi_{i-1}^2 \Lambda_{1\omega_{n_u}}$ when $i > 1$ and where $\phi_{i-1} = \overline{\sigma}\left(W_{2,i-1}(j\omega_{n_u}) P(j\omega_{n_u}) W_{1,i-1}(j\omega_{n_u})\right)$. Denote by $\Lambda_{1\omega_q}^\star$ and $\Lambda_{2\omega_q}^\star$ the values of $\Lambda_{1\omega_q}$ and $\Lambda_{2\omega_q}$, respectively, that achieve the aforementioned minimization at each ω_q.

   (ii) Solve the following optimization problem at each frequency grid-point $\omega_q < \omega_{n_l}$, where $q = n_l - 1, n_l - 2, \ldots, 1$ (here, $|W_{2,i}(j\omega_q)|$ is pinned down to $\left(\Lambda_{2\omega_{n_l}}^\star\right)^{1/2}$ $\forall \omega_q$):
   Minimize $\underline{s}(\omega_q)^{-2}$ such that $\exists \Lambda_{1\omega_q} \in \mathbf{\Lambda_n}$ satisfying (2a), (2c), (2d), and (2f). Note that $\gamma_{\omega_q}^2$ is fixed as $\frac{1}{\bar{\epsilon}^2}$ in (2c), and in (2f), $\Lambda_{1\omega_{n_l}} = \Lambda_{1\omega_{n_l}}^\star$ and $\delta\nu = \log_{10}(\omega_{q+1}) - \log_{10}(\omega_q)$. Denote by $\Lambda_{1\omega_q}^\star$ and $\underline{s}_i(\omega_q)^\star$ the values of $\Lambda_{1\omega_q}$ and $(\underline{s}(\omega_q)^{-2})^{-1/2}$, respectively, that achieve the aforementioned minimization at each ω_q.

   (iii) Solve the following optimization problem at each frequency grid-point $\omega_q > \omega_{n_u}$, where $q = n_u + 1, n_u + 2, \ldots, N$ (here, $|W_{1,i}(j\omega_q)|$ is pinned down to $(\Lambda_{1\omega_{n_u}}^\star)^{-1/2}$ $\forall \omega_q$):
   Minimize $\overline{s}(\omega_q)^2$ such that $\exists\ \Lambda_{2\omega_q} \in \mathbf{\Lambda_m}$ satisfying (2b), (2c), (2e), and (2g). Similarly, $\gamma_{\omega_q}^2$ is fixed 'a priori' as $\frac{1}{\bar{\epsilon}^2}$ in (2c) and $\Lambda_{2\omega_{n_u}} = \Lambda_{2\omega_{n_u}}^\star$ in (2g). Denote by $\Lambda_{2\omega_q}^\star$ and $\overline{s}_i(\omega_q)^\star$ the values of $\Lambda_{2\omega_q}$ and $\left(\overline{s}(\omega_q)^2\right)^{1/2}$, respectively, that achieve the aforementioned minimization at each ω_q.
4. Construct *diagonal* transfer function matrices $W_{1,i}^\star(s)$ and $W_{2,i}^\star(s)$ in $\mathcal{GH}_\infty$ by fitting stable minimum phase transfer functions to each magnitude data on the main diagonal of $(\Lambda_{1\omega_q}^\star)^{-1/2}$ and $(\Lambda_{2\omega_q}^\star)^{1/2}$, where $q = 1, 2, \ldots, N$.
5. Compute $b_{\text{opt}}(W_{2,i}^\star P W_{1,i}^\star)$ as detailed in [19], and let this value be denoted by $\varepsilon_{\text{max},i}^\star$. Furthermore, synthesize a controller $C_{\infty,i}^\star$ that achieves a robust stability margin $b(W_{2,i}^\star P W_{1,i}^\star, C_{\infty,i}^\star) = \varepsilon_{max,i}^\star$ usually using the state-space formula given in [20, Theorem 6.3]. Set $C_i^\star = W_{1,i}^\star C_{\infty,i}^\star W_{2,i}^\star$.
6. Evaluate $\left|(\varepsilon_{\text{max,i}}^\star - \varepsilon_{max,i-1}^\star)\right|$. If this value is very small, for instance 0.01, and has remained this small for the last few iterations, then EXIT; otherwise, return to Step 2. The improvement in the loop-gain at low and high frequencies can alternatively be used as an indicator to exit the algorithm, that is, EXIT if there is 'less significant' improvement in the obtained loop-shape $\underline{s}_i^\star(\omega_q)$ and $\overline{s}_i^\star(\omega_q)$ relative to $\underline{s}_{i-1}^\star(\omega_q)$ and $\overline{s}_{i-1}^\star(\omega_q)$, respectively.

[¶]Note that the controller $C(j\omega_q)$ is replaced by $C_{i-1}^\star(j\omega_q)$ in (2c) for the ith iteration.

DOI: 10.1002/rnc

Outputs from the algorithm

- The optimized robust stability margin $b(P_s, C_\infty)$ obtained in the variable $\varepsilon^\star_{max,i}$,
- The maximized pointwise-in-frequency robust stability margin $\rho_{\omega_q}(P_s, C_{\infty,i-1})$ at mid frequencies obtained in the variable $\left(\sqrt{\gamma^2_{\omega_q,i}}\right)^{-1}$ $\forall \omega_q \in [\omega_{n_l}, \omega_{n_u}]$,
- Smooth diagonal loop-shaping weights $W^\star_{1,i}(s)$ and $W^\star_{2,i}(s)$ that achieve $\varepsilon^\star_{\mathrm{max,i}}$ and also maximize the robust performance, and
- A robust stabilizing controller $C^\star_{\infty,i}(s)$ that achieves $b(W^\star_{2,i} P W^\star_{1,i}, C^\star_{\infty,i}) = \varepsilon^\star_{max,i}$.

Remark 2

Being an ascent algorithm, the following should be noted:

(i) Performance and robustness at low and high frequencies, respectively, are monotonically non-decreasing as i increases, that is, $\underline{s}^\star_{i+1}(\omega_q) \geqslant \underline{s}^\star_i(\omega_q)$ $\forall \omega_q \in [\omega_1, \omega_{n_l})$ and $\overline{s}^\star_{i+1}(\omega_q) \leqslant \overline{s}^\star_i(\omega_q)$ $\forall \omega_q \in (\omega_{n_u}, \omega_N]$.

(ii) Although monotonicity in the optimized value of $b(P_s, C_\infty)$ obtained in the variable $\varepsilon^\star_{max,i}$ cannot be guaranteed as i increases because of the trade-off between robust stability and robust performance, the difference between $\rho_{\omega_q}(P_s, C_{\infty,i-1})$ at mid frequencies and $b(P_s, C_\infty)$ is monotonically non-decreasing, that is, $\frac{1}{\left(\sqrt{\gamma_{\omega_q,i}}^2\right)} \geqslant \varepsilon^\star_{\mathrm{max,i-1}} \forall \omega_q \in [\omega_{n_l}, \omega_{n_u}]$ and $\varepsilon_{\mathrm{max,i}} \geqslant \bar{\epsilon}$ $\forall i$.

(iii) The initial choice of the stabilizing controller, the trade-off involved in the particular problem, and the specified complexity constraints determine the convergence speed of the solution algorithm. Even though this speed varies with the initial choice of the stabilizing controller, there is ample freedom to alter the initial controller at optimization stages 3 and 5 of each iteration because stage 3 allows the controller to change its frequency shape via an optimization of weights and stage 5 optimizes C_∞ completely by maximizing $\varepsilon_{\mathrm{max,i}}$.

(iv) The LMIs at each frequency grid-point $\omega_q \in [\omega_{n_l}, \omega_{n_u}]$ for the mid frequency optimization can be packed together into a single LMI constraint to solve the optimization problem in one go.

(v) For the optimization at each grid point, the number of decision variables is $(m + n + 2i_w)$, where $i_w = 1$ when the optimization is over only one weight and $i_w = 2$ when the optimization is over both weights. The number of decision variables, therefore, increases with the dimension of the nominal plant. However, this number does not depend on the order of the plant.

For the feasibility of the optimization problems at low and high frequencies, an initial stabilizing controller $C^\star_0 = W^\star_{1,0} C^\star_{\infty,0} W^\star_{2,0}$ satisfying $b(W^\star_{2,0} P W^\star_{1,0}, C^\star_{\infty,0}) \geqslant \bar{\epsilon}$ for a given plant P is required in Step 1 of the algorithm. Guidelines for choosing a feasible initial stabilizing controller, that is, W_1, W_2, and C_∞, for a given plant are now provided.

Remark 3

(a) For any given stable plant $P \in \mathscr{RH}_\infty{}^{m\times n}$, the condition $b(W_2 P W_1, C_\infty) > \frac{1}{\gamma}$, where $\gamma > 1$, is always satisfied for the following choice: $C_\infty = 0_{n\times m}$, $W_2 = I_m$, and $W_1 = wI_n$, where $w < \frac{\sqrt{\gamma^2-1}}{||P||_\infty}$. The proof is briefly shown as follows:

For $P \in \mathscr{RH}_\infty$, $C_\infty = 0$ is internally stabilizing. Now, by using the definition of $b(P_s, C_\infty)$ given in (1), where $P_s = W_2 P W_1 = wP$, the following can be written

$$\left\|\begin{bmatrix} wP \\ I \end{bmatrix}\begin{bmatrix} 0 & I \end{bmatrix}\right\|_\infty < \gamma \Leftrightarrow w^2 P^* P + I < \gamma^2 I$$

$$\Leftrightarrow P^* P < \frac{(\gamma^2 - 1)}{w^2} I \Leftrightarrow ||P||_\infty < \frac{\sqrt{\gamma^2 - 1}}{w}.$$

DOI: 10.1002/rnc

(b) Given that the plant P is strictly positive real, let $W_1 = W_2 = I_n$ and $C_\infty = -I_n$. Then, the feedback interconnection of Figure 2(a) is internally stable (by invoking passivity theorem [21]) and $\gamma \leqslant \sqrt{2}$ [22, 23].

(c) For an unstable plant P, the algorithm given in Section 3 can be used to synthesize weights and controller that achieve $b(P_s, C_\infty) \geqslant 0.3$ without placing any restriction on the required loop-shape, that is, (2a) and (2b) are inactive.

7. NUMERICAL EXAMPLE

We consider a MIMO design example for pitch control of a highly maneuverable airplane (see [24, 25] for more information). The model is taken from the highly maneuverable aircraft technology vehicle data [25], a scaled, remotely piloted flight model with poles and zeros located at $s = -2.2321 \pm j3.3779, -0.0442 \pm j0.2093$, and $s = -0.0226$, respectively. The scaled nominal open-loop plant is given in state-space form as shown next, and the singular-value plot is shown in Figure 3.

$$P = \left[\begin{array}{cccc|cc} -0.0226 & -36.6 & -18.9 & -32.1 & 0 & 0 \\ 0 & -1.9 & 0.983 & 0 & -0.414 & 0 \\ 0.0123 & -11.7 & -2.63 & 0 & -77.8 & 22.4 \\ 0 & 0 & 1 & 0 & 0 & 0 \\ \hline 0 & 57.3 & 0 & 0 & 0 & 0 \\ 0 & 0 & 0 & 57.3 & 0 & 0 \end{array}\right]$$

For the purpose of illustration and justification of the proposed algorithm, the same design objectives specified in [24] are used: disturbance rejection up to 1 rad/s in the presence of substantial plant uncertainty higher than 100 rad/s and a desired closed-loop bandwidth of approximately 10 rad/s.

In view of the aforementioned specifications, ω_l and ω_u are chosen as 12 rad/s and 160 rad/s, respectively. $\bar{\epsilon}$ is fixed at 0.3 for the optimization problems in low frequency and high frequency regions, thus allowing unstructured plant perturbation $||\Delta||_\infty < 0.3$. The solution algorithm formulated in the previous section is now invoked to simultaneously synthesize weights W_1 and W_2 and a stabilizing controller C_∞ that maximize the loop-gain, improve the pointwise-in-frequency

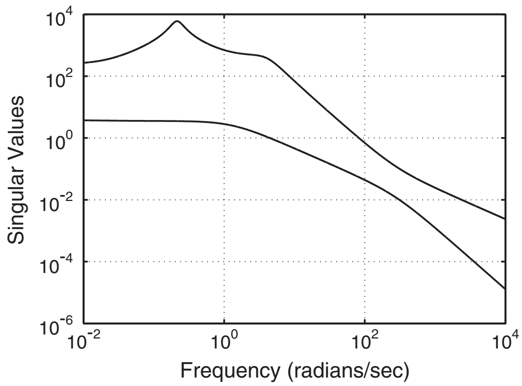

Figure 3. Singular-value plot of the scaled nominal plant.

DOI: 10.1002/rnc

robust stability margin, and minimize the loop-gain at low, mid, and high frequencies, respectively. Because a controller satisfying $b(P_s, C_\infty) \geqslant 0.3$ is needed to initialize the solution algorithm, the synthesized controller using the $\mathscr{H}_\infty$ LSDP in [24] with $b(P_s, C_\infty)$ of 0.4306 is used. The guideline given in Remark 2(a) can also be used to synthesize a feasible stabilizing controller for this plant. For instance, $C_\infty = 0_2$, $W_1 = 0.001 I_2$, and $W_2 = I_2$ for the stable highly maneuverable aircraft technology vehicle with $||P||_\infty = 1.37 \times 10^3$ yields $b(P_s, C_\infty) = 0.69$.

Because of simple design specifications, the frequency functions $\underline{w}_i$, $\overline{w}_i$, k_i, and g_i that confine the singular values, the condition number, and the gradient of $W_i (i = 1, 2)$ are chosen as 10^{-5}, 10^5, 5, and 60 dB/dec, respectively. Two hundred equally spaced frequency points on a logarithmic scale between $\omega_1 = 10^{-2}$ rad/s and $\omega_N = 10^4$ rad/s are used to formulate the optimization problems in Step 3, and four iterations were required for the convergence of the algorithm, which took less than 12 min.

Figure 4(a) shows the evolution of $\underline{s}(\omega_q)$ and $\overline{s}(\omega_q)$ at low and high frequencies, respectively, where the loop-gain of the compensated system is maximized at low frequencies and minimized at high frequencies. The closed-loop performance is hence improved, and this is also confirmed in the singular values of the correspondingly achieved loop-shape P_s shown in Figure 4(b). Moreover, the singular values of the output sensitivity and input complementary sensitivity functions respectively shown in Figure 5(a) and 5(b) further support the claim that the closed-loop performance of the system is improved using the proposed algorithm when compared with the design in [24]: the output sensitivity function, indicator of nominal performance, is lower at low frequencies, whereas the

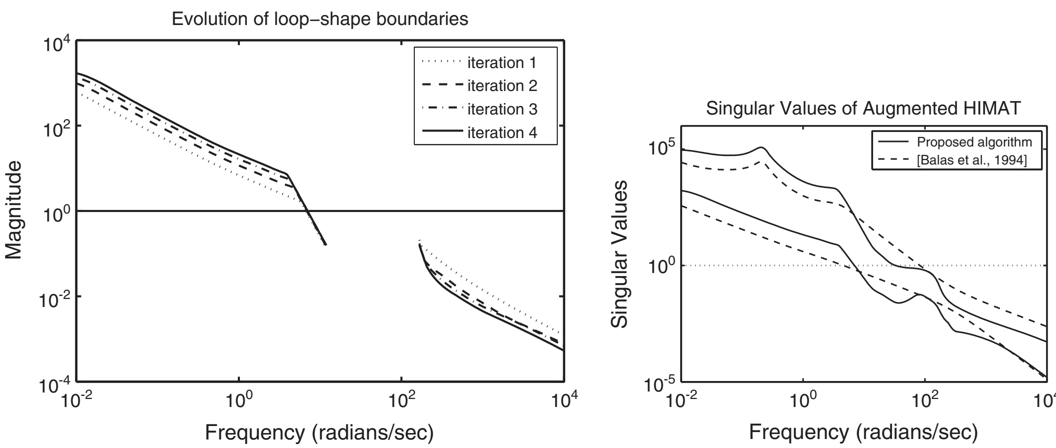

Figure 4. (a) Loop-shape boundaries and (b) singular values of the augmented system. HIMAT, highly maneuverable aircraft technology.

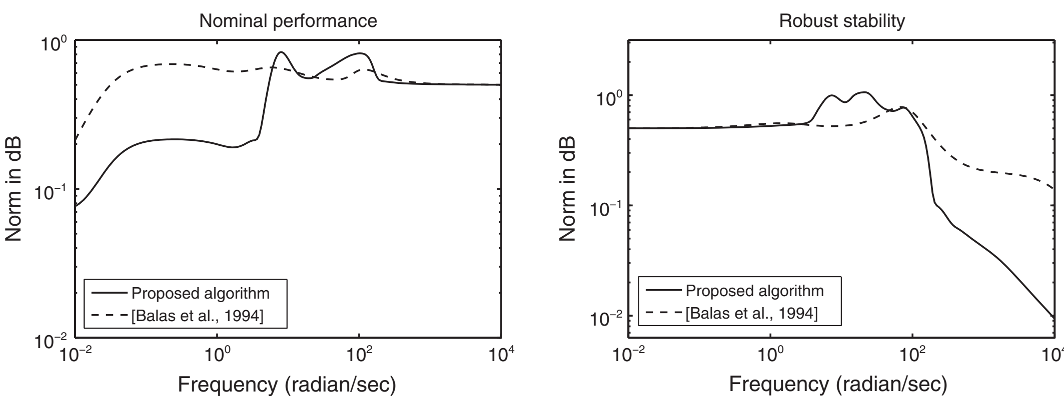

Figure 5. (a) Output sensitivity function and (b) input complementary sensitivity function.

DOI: 10.1002/rnc

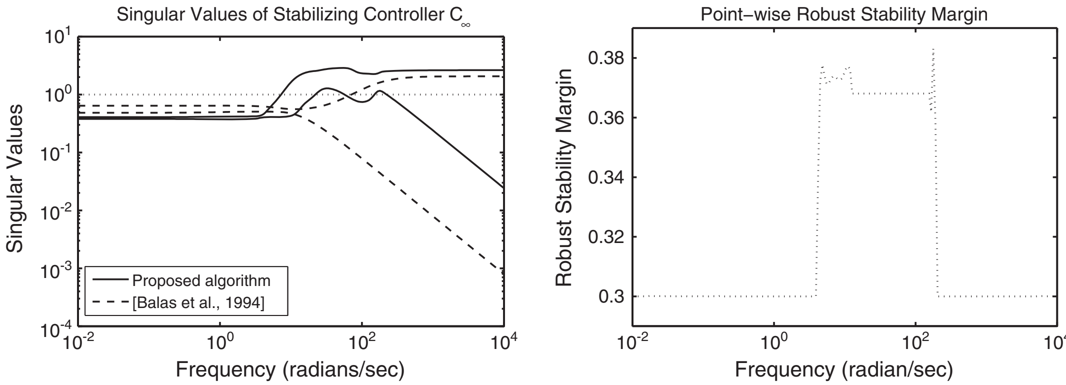

Figure 6. (a) Robust stabilizing controller and (b) pointwise robust stability margin.

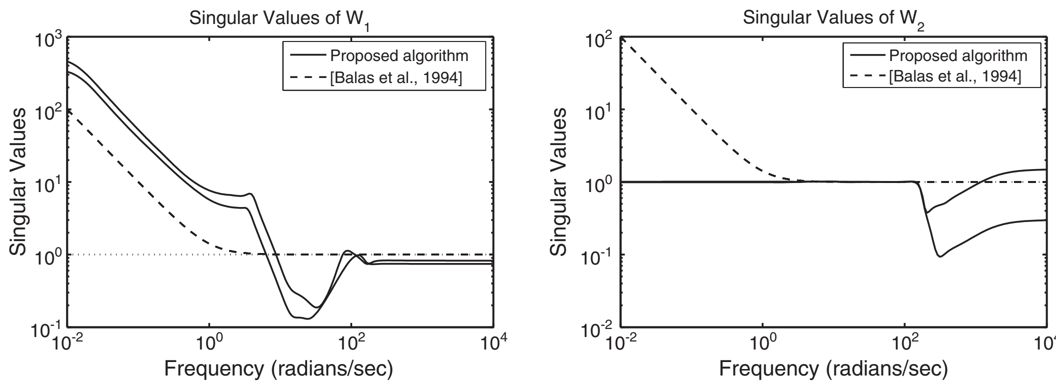

Figure 7. (a) Pre-compensator W_1 and (b) post-compensator W_2.

input complementary sensitivity function, an indicator of the closed-loop robust stability, is lower at high frequencies. Note that the design indicator for the mid frequency region is the pointwise-in-frequency robust stability margin, which, thus, explains why the sensitivity values are higher in this region. It should also be noted that the lightly damped modes at mid frequencies (which explains the shape of the sensitivity functions in this region) are detected and retained by the algorithm while maximizing the robust stability margin.

The robust stability margin obtained from the design was 0.3548, which is an indicator of a decent design. To illustrate the effect of the optimization problem at mid frequencies, the plot of the pointwise-in-frequency robust stability margin using the penultimate controller is shown in Figure 6(b). A minimum $\rho_{\omega_q}(P_s, C_\infty)$ of 0.3680 was obtained in the mid frequency region before the final controller synthesis. The singular values of the simultaneously synthesized robust stabilizing controller C_∞ and the synthesized weights are shown in Figures 6(a), 7(a), and 7(b), respectively. The order of W_1, as well as W_2, is 13, and this can be reduced using model reduction techniques given in [13], if required. Also, the condition numbers of the weights are less than 5 at all frequencies, which is typically considered good.

8. CONCLUSION

In contrast to the conventional $\mathscr{H}_\infty$ LSDP and, in fact, most design approaches, a different design paradigm has been introduced. The proposed paradigm casts optimization problems in a systematic manner such that the desired closed-loop design objectives at low, mid, and high frequencies are captured. The resulting solution facilitates the simultaneous synthesis of loop-shaping weights and a robust stabilizing controller that maximize the robust performance for a guaranteed level of robust stability margin in $\mathscr{H}_\infty$ loop-shaping control. This work, thus, answers the question of the best achievable performance for a guaranteed level of stability margin in a feedback control system. The solution algorithm is computationally efficient as the optimization problems are formulated in LMI framework and are easily implementable using an available LMI toolbox.

ACKNOWLEDGEMENTS

Many thanks to Sönke Engelken and Zhuoyue Song of the Control Systems Centre, The University of Manchester, for their valuable and helpful comments. Also, the financial support of the Engineering and Physical Sciences Research Council and the Royal Society is gratefully acknowledged.

REFERENCES

1. McFarlane D, Glover K. A loop-shaping design procedure using $\mathscr{H}_\infty$ synthesis. *IEEE Transactions on Automatic Control* 1992; **37**(6):759–769.
2. Doyle J, Smith R, Enns D. Control of plants with input saturation nonlinearities. *Proceedings of the American Control Conference*, Arizona, 1987; 1034–1039.
3. Kothare M. Control of systems subject to constraints. *PhD thesis*, California Institute of Technology, 1997.
4. Weston P, Postlethwaite I. Linear conditioning for systems containing saturating actuators. *Automatica* 2000; **36**(9):1347–1354.
5. Roberts J, Roberts T. Use of the butterworth low-pass filter for oceanographic data. *Journal of Geophysical Research* 1978; **83**:5510–5514.
6. Lanzon A. Weight optimisation in $\mathscr{H}_\infty$ loop-shaping. *Automatica* 2005a; **41**(1):1201–1208.
7. Osinuga M, Patra S, Lanzon A. Smooth weight optimization in $\mathscr{H}_\infty$ loop-shaping design. *Systems and Control Letters* 2010; **59**:663–670.
8. Gu K. Designing stabilizing control of uncertain systems by quasiconvex optimization. *IEEE Transactions on Automatic Control* 1994; **39**(1):127–131.
9. Vinnicombe G. *Uncertainty and Feedback: $\mathscr{H}_\infty$ Loop-shaping and V-gap Metric*. Imperial College Press: London, United Kingdom, 2001.
10. Tsai M, Geddes E, Postlethwaite I. Pole-zero cancellations and closed-loop properties of an $\mathscr{H}_\infty$ mixed sensitivity design problem. *Proceedings of IEEE Conference on Decision and Control*, Honolulu, HI, USA, 1990; 1028–1029.
11. Hyde R. *$\mathscr{H}_\infty$ aerospace control design-a VSTOL flight application*, In advances in industrial control series. Springer: Berlin, 1995.
12. Papageorgiou G, Glover K. A systematic procedure for designing non-diagonal weights to facilitate $\mathscr{H}_\infty$ loop shaping. *Proceedings of IEEE Conference on Decision and Control*, San Diego, CA, US, 1997; 2127–2132.
13. Zhou K, Doyle J, Glover K. *Robust and Optimal Control*. Prentice Hall: Englewood Cliffs, NJ, 1996.
14. Lanzon A, Cantoni M. On the Formulation and Solution of Robust Performance Problems. *Automatica* 2003; **39**(10):1707–1720.
15. Lanzon A. Pointwise in frequency performance weight optimization in μ-synthesis. *International Journal of Robust and Nonlinear Control* 2005b; **15**(4):171–198.
16. Pettazzi L, Lanzon A. Systematic design of optimal performance weight and controller in mixed-μ synthesis. *Proceedings of IFAC World Congress*, Seoul, Korea, 2008; 7814–7819.
17. Skogestad S, Postlethwaite I. *Multivariable Feedback Control: Analysis and Design*. John Wiley and Sons: New York, NY, USA, 1998.
18. Glover K, Vinnicombe G, Papageorgiou G. Guaranteed multi-loop stability margins and the gap metric. *Proceedings of IEEE Conference on Decision and Control*, Sydney, Australia, 2000; 4084–4085.
19. Glover K, McFarlane D. Robust stabilization of normalized coprime factor plant descriptions with $\mathscr{H}_\infty$-bounded uncertainty. *IEEE Transactions on Automatic Control* 1989; **34**(8):821–830.
20. Glover K. All optimal hankel-norm approximations of linear multivariable systems and their $\mathscr{L}_\infty$-error bounds. *International Journal of Control* 1984; **39**(6):1115–1193.
21. Khalil H. *Nonlinear Systems*, Vol. 2. Prentice Hall: Upper Saddle River, NJ 07458, 2007.
22. McFarlane D, Glover K. *Lecture Notes in Control and Information Sciences: Robust Controller Design Using Normalized Coprime Factor Plant Descriptions*, Vol. 138. Springer-Verlag: Heidelberg, Germany, 1990.
23. Iwasaki T, Hara S, Yamauchi H. Dynamical system design from a control perspective: Finite frequency positive-realness approach. *IEEE Transactions on Automatic Control* 2003; **48**(8):1337–1354.
24. Balas J, Doyle J, Glover K, Packard A, Smith R. *μ-analysis and Synthesis Toolbox User's Guide*. The MathWorks Inc.: Natick, MA, 1994.
25. Safonov M, Whitmoyer R. Feedback properties of multivariable systems: the role and use of the return difference matrix. *IEEE Transactions on Automatic Control* 1981; **AC-26**(1):47–65.